arXiv:1604.08519v1 [cond-mat.mes-hall] 28 Apr 2016

Tailoring the core electron density in modulation-doped Core-Multi-Shell nanowires

Fabrizio Buscemi[1], **Miquel Royo**[2,3], **Guido Goldoni**[1,4], **Andrea Bertoni**[4]

[1]Department of Physics, Informatics, and Mathematics, University of Modena and Reggio Emilia, Via Campi 213/A, 41125 Modena, Italy
[2]Departament de Química Física i Analítica, Universitat Jaume I, Castelló, Spain
[3]Institut de Ciència de Materials de Barcelona ICMAB-CSIC, Campus de Bellaterra, Barcelona, Spain
[4]Centro S3, Istituto Nanoscienze - CNR, Modena, Italy

E-mail: andrea.bertoni@nano.cnr.it

Abstract. We show how a proper radial modulation of the composition of core-multi-shell nanowires critically enhances the control of the free-carrier density in the high-mobility core with respect to core-single-shell structures, thus overcoming the technological difficulty of fine tuning the remote doping density. We calculate the electron population of the different nanowire layers as a function of the doping density and of several geometrical parameters by means of a self-consistent Schrödinger-Poisson approach: Free carriers tend to localize in the outer shell and screen the core from the electric field of the dopants.

Submitted to: *Nanotechnology*

1. Introduction

Semiconductors nanowires (NWs) have the potential to become a key component of next-generation ultrafast electronic nanodevices such as high mobility transistors, [1, 2] light-emitting diodes, [3], wavelength-controlled lasers [4] and photovoltaic cells. [5] In particular, controlled epitaxial lateral overgrowth enabled the development of radial modulation doping techniques, a crucial step towards high-mobility NW devices [6].

High conductivity GaAs NWs with a large aspect ratio and a diameter of few nanometers have been demonstrated. [7] With remote doping, the conductive core of the NW is spatially separated from the dopants, reducing carrier scattering by impurities. However, the controlled incorporation of dopants in NWs is still challenging [8], with poor control of the free-carrier density, the latter being a critical parameter to calibrate the electronic characteristics of devices. Indeed, a core electron population which is weakly sensitive to dopant concentration is a key feature for the application of NWs in high performance electronics.

In this article, we show that a proper radial modulation of the semiconductor NW with an additional conductive layer, a so-called quantum well tube (QWT), will critically decrease the impact of doping uncertainty on the free-electron density in the high conductive NW core. To analyse the impact of compositional parameters on free-carrier concentration and localization we use quantum self-consistent calculations as well as a semi-classical approximation for comparison.

Radial heterostructures have been grown both as core-single-shell NW (SSNW) structures and as core-multi-shell NW (MSNW) structures. In the latter case, one or multiple conductive QWTs can be grown around the NW core. The scheme of an hexagonal MSNW with two insulating AlGaAs shells is shown in Fig. 1(a) and (b). Different doping levels result in the formation and localization of free carriers gas at the facets, corners or in the center of the hexagonal NW core. [9, 8, 10, 11] Additionally, in MSNWs carriers can be confined in the QWT wrapped around the core. [6] The charge accumulating in the outer shells will eventually screen the electrostatic field generated by remote doping, reducing its effect on the population of the core.

2. Method

Our prototypical heterostructure is a n-doped GaAs/AlGaAs MSNWs with hexagonal cross section. However, our results are not limited to this kind of samples since they are not linked to a specific material or symmetry of the NW. To obtain the free-electron density distributions, we use a self-consistent Schrödinger-Poisson approach. [12, 9, 13, 14, 15] Within an effective mass, single band approximation, assuming translational invariance along the NW growth z-axis, quantum states are given by the 2D Schrödinger equation

$$\left[-\frac{\hbar^2}{2}\nabla_{\mathbf{r}}\frac{1}{m^*(\mathbf{r})}\nabla_{\mathbf{r}} + E_C(\mathbf{r}) - eV(\mathbf{r})\right]\psi_n(\mathbf{r}) = E_n\psi_n(\mathbf{r}), \tag{1}$$

where $\mathbf{r} = (x, y)$ is the 2D coordinate, m^* is the material-dependent effective mass of the electron, E_C and V are the local conduction band edge and the electrostatic potential generated by free electrons and dopants, respectively. Exchange and correlation effects are not included since they are found to be negligible in the devices under consideration. [13, 9] The box integration method on a triangular mesh with hexagonal elements is used to solve Eq. 1 [9, 14] on an hexagonal domain.

Once the wave functions $\psi_n(\mathbf{r})$ and subband energies E_n are obtained, the electron density $n(\mathbf{r})$ at temperature T is computed from subband population with the Fermi distribution,

$$n(\mathbf{r}) = 2\sum_n |\psi_n(\mathbf{r})|^2 \sqrt{\frac{m^* k_B \mathrm{T}}{2\pi\hbar^2}} \mathcal{F}_{-\frac{1}{2}}\left(\frac{E_\mathrm{F} - E_n}{k_B \mathrm{T}}\right) \tag{2}$$

where E_F denotes the Fermi level and $\mathcal{F}_j(x) = \frac{1}{\Gamma(j+1)} \int_0^\infty \frac{t^j dt}{e^{t-x}+1}$ is the complete Fermi-Dirac integral of order j resulting from the integration of the parabolic dispersion along the free axis.

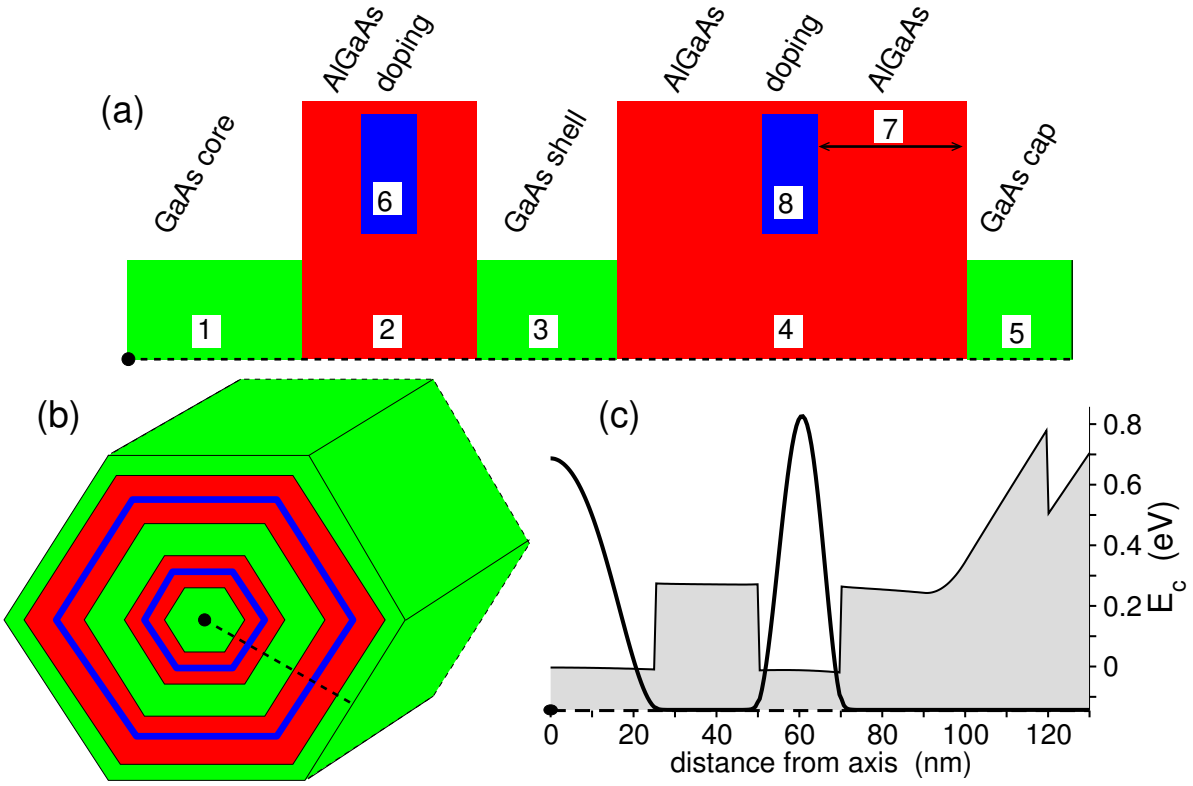

Figure 1. Schematics of the radial composition (a) and cross-section (b) of a GaAs/AlGaAs MSNW. In (a) composition is represented from the NW center (left) to the outer shell (right). The height of each layer represents E_C. Numeric labels refer to layer widths in Tab. 1. (c) Example of the self-consistent potential (filled area) and electron density (solid line) along the dashed line of panel (b), for sample M_1 (see Tab. 1).

The electrostatic potential $V(\mathbf{r})$ due to the electrons and ionized dopants is obtained from the Poisson equation

$$\nabla_{\mathbf{r}} \left[\epsilon_r(\mathbf{r}) \nabla_{\mathbf{r}} V(\mathbf{r})\right] = -\frac{e}{\epsilon_0}[\rho_D(\mathbf{r}) - n(\mathbf{r})], \tag{3}$$

where $\epsilon_r(\mathbf{r})$ is the position-dependent dielectric constant, ϵ_0 is the vacuum permittivity, and $\rho_D(\mathbf{r})$ is the ionized donor density. Dirichlet boundary conditions are used to solve Eq. 3. $V(\mathbf{r})$ is inserted into Eq. 1 and the whole procedure is repeated until self-consistency is reached, i.e., the relative variation of the electron density between successive iterations is lower than 10^{-3} at any point of the domain. Finally, the free-carrier linear charge density n_{l} of the NW is calculated as $n_{\mathrm{l}} = \int_A n(\mathbf{r}) d\mathbf{r}$, with A the NW cross section.

To assess the impact of the quantum states in these structures, we also compute the linear charge density with a semiclassical approach, where electron states are approximated by plane waves $\psi \propto \exp\left[i\left(k_x x + k_y y + k_z z\right)\right]$ with parabolic dispersion, and the wave vectors in the x and y directions are integrated over. The electron density is now obtained from [12]

$$n_{\mathsf{sc}}(\mathbf{r}) = 2\left(\frac{m^* k_B \mathrm{T}}{2\pi\hbar^2}\right)^{3/2} \mathcal{F}_{\frac{1}{2}}\left(\frac{E_{\mathrm{F}} - E_C(\mathbf{r}) + eV(\mathbf{r})}{k_B \mathrm{T}}\right). \tag{4}$$

$n_{\mathsf{sc}}(\mathbf{r})$ is then inserted in the Poisson equation 3 in place of $n(\mathbf{r})$, and the procedure is iterated like in the fully quantum approach. Clearly, since the solution of (1) is not required, the semiclassical approach is much faster.

3. System

We simulated different prototype structures, with the general scheme shown in Fig. 1. The geometrical parameters of the investigated samples are reported in Tab. 1. Calculations are performed at T = 4 K, and the GaAs and AlGaAs band gaps are taken as 1.43 eV and 1.858 eV, respectively, with the Fermi level E_{F} set at the mid-gap value of GaAs. [16] Other material parameters are m^*(GaAs) = 0.062, ϵ_r(GaAs) = 13.18, m^*(AlGaAs) = 0.092, and ϵ_r(AlGaAs) = 12.24. [16]

In the following, we first analyse the multi-shell structure M_1, where the effects we want to emphasize are prominent. Then, we show that similar SSNW samples (S_1 and S_2), or a double-doped MSNW sample, do not present the screening effect.

(nm)	Δ_1	Δ_2	Δ_3	Δ_4	Δ_5	Δ_6	Δ_7	Δ_8
M_1	25	25	20	50	10	0	20	10
S_1	25	0	0	95	10	0	20	10
S_2	25	0	0	95	10	0	65	10
M_2	25	25	20	50	10	10	20	10

Table 1. Geometrical parameters of the MSNW (M_1 and M_2) and SSNW (S_1 and S_2) structures simulated. The widths Δ_1-Δ_8 refer to the labelling in Fig. 1(a).

4. MSNW M_1

Figure 2(c) shows the linear free-electron density of structure M_1, obtained from the quantum (lines) and semiclassical (dots) approaches *vs* the donor density ρ_D, uniformly distributed in a 10-nm-thick layer (Δ_6) in the outer AlGaAs barrier. In agreement with other works, [3, 9, 7], we find a threshold doping density ($\sim 1.55 \times 10^{18}$ cm^{-3}) below which no free-electron charge is obtained. Above this threshold, the linear electron densities in the GaAs core and shell increase almost linearly with ρ_D.

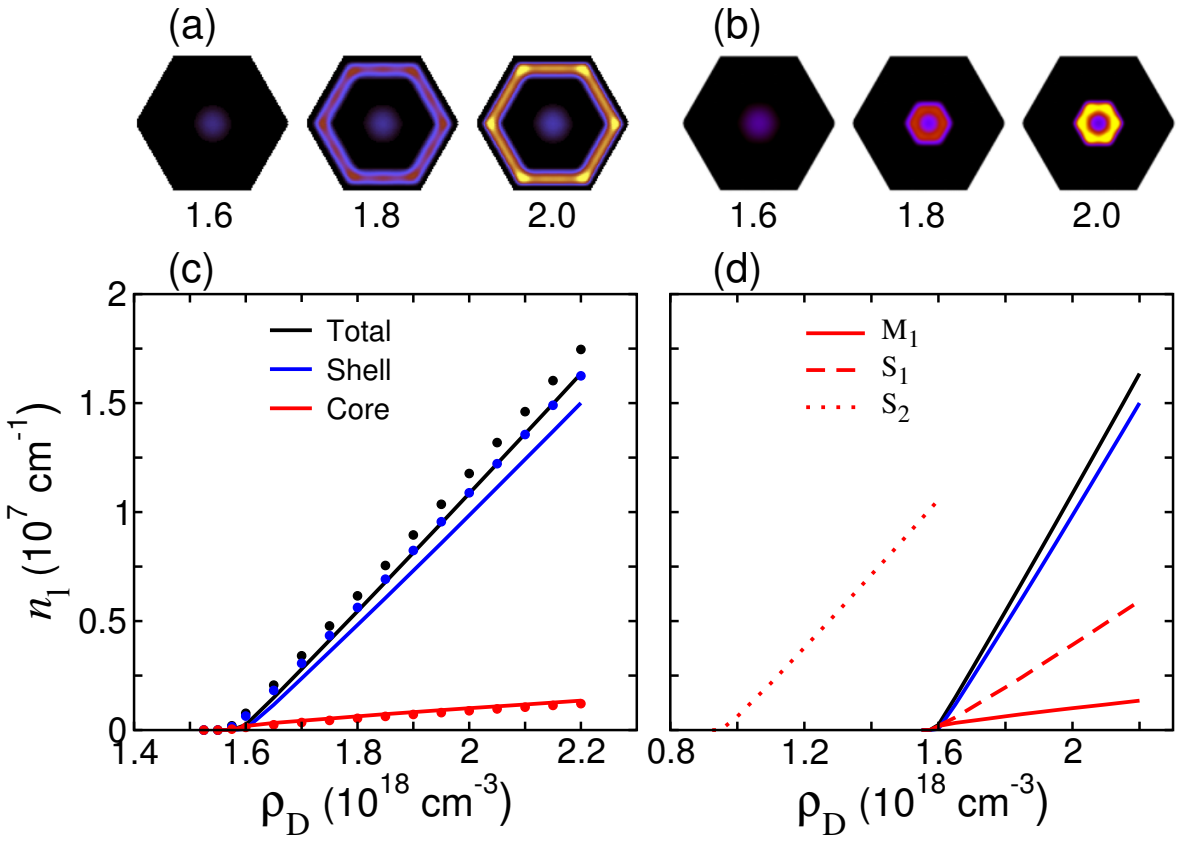

Figure 2. Electron gas distribution in samples M_1 (a) and S_1 (b) at three doping densities. Quantum effects are included. (c) Linear charge density n_l for sample M_1, obtained from the fully quantum approach (solid lines) and the semiclassical approach (dots) *vs* the donor density ρ_D . The three curves report n_l in the core (red), in the shell (green) and the total charge density (black). (d) Linear charge density of samples S_1 (dashed) and S_2 (dotted) compared with M_1 (solid lines), where all charge is located in the core. In M_1 the charge in the core is much less sensitive to the doping level.

Charge localization is sensitive to doping concentration. At low doping $\rho_D = 1.6 \times 10^{18}$ cm^{-3}, just above the threshold (left panel of Fig. 2(a)), the GaAs core starts to be populated and the charge is distributed with an isotropic circular symmetry. As ρ_D increases, only a small fraction of the additional free charge accumulates in the core, while most free electrons fill the outer QWT. This is shown, e.g., in the central panel of Fig. 2(a) at $\rho_D = 1.8 \times 10^{18}$ cm^{-3}, where electrons in the shell form a quasi-

uniform sixfold bent 2D gas. At even larger doping, most of the excess free charge still accumulates in the outer shell, but now it tends to form six quasi-1D channels at the QWT bends, due to the larger area available and the sharper bending of the self-consistent field stemming from the repulsive Coulomb potential. This is shown in the right panel of Fig. 2(a), with $\rho_D = 2.0 \times 10^{18}$ cm^{-3}. Being the amount of free charge in the GaAs QWT much larger than the one confined in the core, *it screens the electrostatic field generated by dopants in the central region.* As a consequence, the core electron concentration is weakly affected by the level of doping, as can be gathered from the red curve of Fig. 1(c).

Figure 2 also shows that the results of the fully quantum approach and the semiclassical approch exhibit the same qualitative behaviour, with essentially the same density in the core, and with the density in the GaAs QWT slightly overestimated by the semiclassical approach, due to the lack of quantum confinement effects which shifts the energy subbands upward.

5. Comparison with SSNW S_1 and S_2

To clarify the effect of the presence of the internal AlGaAs layer Δ_2, we repeated the simulations for two SSNWs with composition and dimension identical to M_1, but with $\Delta_2 = 0$. These two samples, namely S_1 and S_2, are designed with different position of the doping layer: in S_1 (S_2) its distance from the outer (inner) GaAs layer is the same as in M_1. The comparison with M_1 is shown in Fig. 2(d). As expected, samples S_1 and S_2 are also populated above a threshold density, which depends on Δ_7, with n_l increasing linearly with doping. Since there is no QWT to accomodate additional charges, charge density in the core can easily reach $\sim 10^7$ cm^{-1} and it is very sensitive to the donor density. Indeed, the conduction band in the central region is significantly bent by the dopants field. The charge distribution in the cross-section of S_1 is illustrated in Fig. 2(b) for three doping densities. At the higher doping level, the free electrons in the core rearrange into a ring-shaped distribution,[9, 17, 18] yet keeping a steep linear trend with doping concentration. To be quantitative, for example, in SSNW S_2 a change in ρ_D of 0.2×10^{18} cm^{-3} (from 1.0×10^{18} to 1.2×10^{18} cm^{-3}) leads to a variation of n_l of about 500% (from 0.62×10^6 to 3.78×10^6 cm^{-1}), while the same doping span (from 1.8×10^{18} to 2.0×10^{18} cm^{-3}) in MSNW M_1 changes n_l of just 60% (from 0.62×10^6 to 1×10^6 cm^{-1}).

6. Effect of shells thickness and doping position

Having assessed that in MSNWs most of the charge localizes in the QWT and screens the ionized dopants, we next investigate the impact of the thickness of the inner barrier, of the well width, and of the doping layer position on the accumulated charge. Accordingly, we vary parameters Δ_2, Δ_3, Δ_7 in sample M_1, while keeping fixed all other parameters. The total MSNW diameter is varied accordingly.

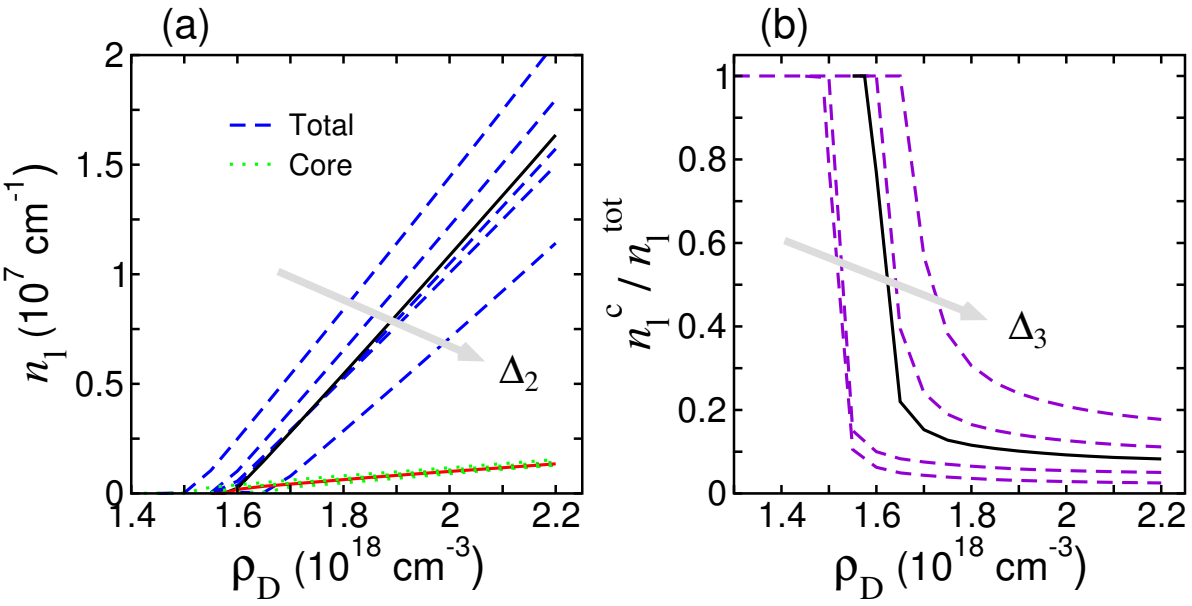

Figure 3. (a) Linear charge density n_1 in the whole NW (blue dashed lines) and in the core (green dotted lines) *vs* donor density ρ_D for $\Delta_2 = 10$, 15, 20, 27, 30 nm. The gray arrow indicates decreasing values of Δ_2. Vallues for the original MSNW M_1, with $\Delta_2 = 25$ nm is reported with solid lines for easy of comparison. (b) Ratio between the core and the total charge density for $\Delta_3 = 10$, 15, 25, 30 nm. The reference structure M_1, with $\Delta_3 = 20$ nm is reported with solid lines for easy of comparison.

Figure 3(a) shows that the distance Δ_2 controls the doping threshold by a simple volume effect. For given doping density a smaller Δ_2 implies a smaller surface of the hexagonal layer occupied by dopants. Therefore a larger density is needed to accumulate the charge. Note that the carrier density in the core is practically independent of Δ_2, and the screening effect is always present.

Decreasing the GaAs well Δ_3 has a similar effect on the threshold. However, the reduction of the screening shell also decreases the amount of charge accumulated in the QWT and the screening effect. Indeed, Fig. 3(b) shows that the ratio between the core and the total linear density increases for smaller Δ_3. So, in order for the screening to be effective and, at the same time, to have a significant charge in the core, the GaAs layer thickness must be properly tailored, as in structure M_1.

The displacement of the 10 nm doping layer inserted in Δ_4, has a remarkable effect. As it moves outwards (Δ_7 decreases) a larger ρ_D is needed to bend the conduction band below the Fermi level. This is shown in Fig. 4(c), with the threshold doping moving to the right as Δ_7 decreases. The effect is stronger for the QWT than for the core, due to their different distance from the doping layer. As a consequence, while the total free-charge density curve becomes less steep, the slope of the core density is unchanged.

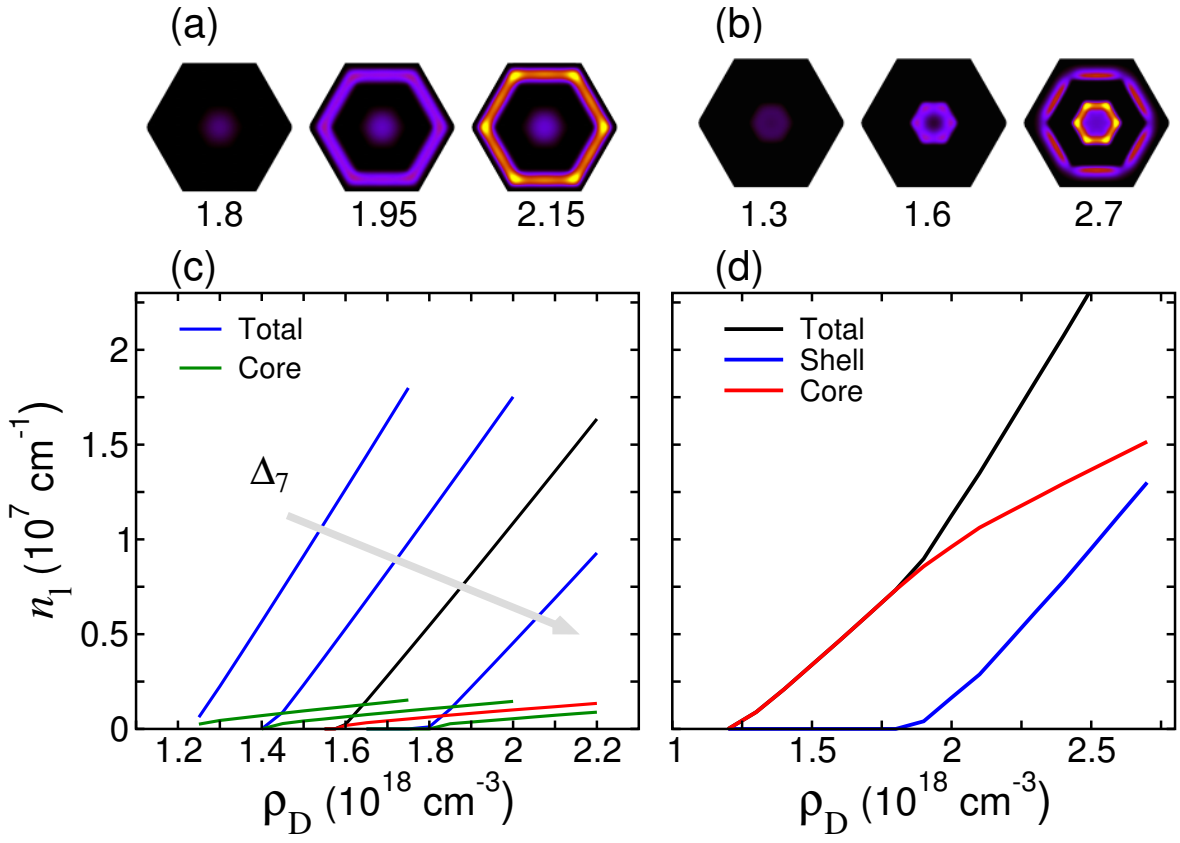

Figure 4. (a)-(b) Electron gas distribution in M_1 with $\Delta_7 = 15$ nm, and in M_2, respectively, at three densities of doping. (c) Linear charge density n_1 against donor density for M_1 with $\Delta_7 = 15$, 20, 25, 30 nm. The gray arrow indicates decreasing values of Δ_7. (d) Linear charge density of M_2, with two doping layers.

7. MSNW M_2

Finally, we investigate sample M_2, where donors are uniformly distributed in *two* 10 nm layers placed in the two AlGaAs barriers. The linear free-electron density *vs* ρ_D is shown in Fig. 4(d) and exhibits two linear regimes, with an abrupt change of slope. In the lower density regime (from 1.22×10^{18} to 1.8×10^{18} cm^{-3}), free electrons localize only the core region. At densities $\rho_D > 1.8 \times 10^{18}$ free carriers start to populate the GaAs shell. The spatial distribution of the electron gas shows peculiar localization patterns, as displayed in Fig. 4(b). At low density, the free electron gas is distributed in the center of the core (left panel). As ρ_D increases, a ring-shaped distribution starts to form, with most of the charge localized on the heterojunction at the edges of the core. For larger dopings, when the QWT start to fill, free electrons localize at the facets of the outer GaAs/AlGaAs interface, forming six separated 2DEG strips. This also affects the core density, whose slope deviates from the low-doping regime. A similar emergence of six almost planar electron gases at the hexagon facets has already been obtained in p-doped MSNWs at low density. [9, 8, 19]

8. Conclusions

In conclusion, we showed how the inclusion of a QWT in MSNWs can strongly decrease the effect of doping level uncertainty on the linear free-electron density of the high-mobility core, yet keeping the ability to populate it with a given density of carriers. We showed numerically that the charge accumulating in the external shell mostly screens the doping electrostatic field in the core for a vast range of shells and doping configurations. This property could make MSNWs better candidates for NW-based high-mobility electronic devices.

Acknowledgements

Numerical simulations were performed at CINECA within the Iscra C project MPL-CSNW. We acknowledge partial financial support from University of Modena and Reggio Emilia, with Grant "Nano- and emerging materials and systems for sustainable technologies." MR acknowledges UJI project P1-1B2014-24, MINECO project CTQ2014-60178-P, Beatriu de Pinos program 2014 BP-B 00101.

References

[1] Cui Y, Zhong Z, Wang D, Wang W U and Lieber C M 2003 *Nano Letters* **3** 149–152
[2] Viti L, Vitiello M, Ercolani D, Sorba L and Tredicucci A 2012 *Nanoscale Research Letters* **7** 159 ISSN 1556-276X
[3] Tomioka K, Motohisa J, Hara S, Hiruma K and Fukui T 2010 *Nano Letters* **10** 1639–1644
[4] Qian F, Gradeak S, Li Y, Wen C Y and Lieber C M 2005 *Nano Letters* **5** 2287–2291
[5] Czaban J A, Thompson D A and LaPierre R R 2009 *Nano Letters* **9** 148–154
[6] Funk S, Royo M, Zardo I, Rudolph D, Morkötter S, Mayer B, Becker J, Bechtold A, Matich S, Döblinger M, Bichler M, Koblmüller G, Finley J J, Bertoni A, Goldoni G and Abstreiter G 2013 *Nano Letters* **13** 6189–6196
[7] Sladek K, Klinger V, Wensorra J, Akabori M, Hardtdegen H and Grtzmacher D 2010 *Journal of Crystal Growth* **312** 635 – 640 ISSN 0022-0248
[8] Jadczak J, Plochocka P, Mitioglu A, Breslavetz I, Royo M, Bertoni A, Goldoni G, Smolenski T, Kossacki P, Kretinin A, Shtrikman H and Maude D K 2014 *Nano Letters* **14** 2807–2814
[9] Bertoni A, Royo M, Mahawish F and Goldoni G 2011 *Phys. Rev. B* **84**(20) 205323
[10] Morkötter S, Jeon N, Rudolph D, Loitsch B, Spirkoska D, Hoffmann E, Döblinger M, Matich S, Finley J J, Lauhon L J, Abstreiter G and Koblmüller G 2015 *Nano Letters* **15** 32953302
[11] Rosdahl T O, Manolescu A and Gudmundsson V 2015 *Nano Letters* **15** 254–258
[12] Datta S 2005 *Quantum Transport: Atom to Transistor* (Cambridge University Press) ISBN 9780521631457
[13] Wong B M, Leonard F, Li Q and Wang G T 2011 *Nano Letters* **11** 3074–3079
[14] Royo M, Bertoni A and Goldoni G 2013 *Phys. Rev. B* **87**(11) 115316
[15] Royo M, Segarra C, Bertoni A, Goldoni G and Planelles J 2015 *Phys. Rev. B* **91**(11) 115440
[16] Levinshtein M, Rumyantsev S and Shur M 1996 *Handbook Series on Semiconductor Parameters* (World Scientific Publishing)
[17] Sitek A, Serra L m c, Gudmundsson V and Manolescu A 2015 *Phys. Rev. B* **91**(23) 235429
[18] Ballester A, Planelles J and Bertoni A 2012 *Journal of Applied Physics* **112** 104317
[19] Buscemi F, Royo M, Bertoni A and Goldoni G 2015 *Phys. Rev. B* **92**(16) 165302